

# The hidden spin-momentum locking and topological defects in unpolarized light fields

Peng Shi<sup>1, #, \*</sup>, Min Lin<sup>1, #</sup>, Xinxin Gou<sup>1, #</sup>, Luping Du<sup>1, \*</sup>, Aiping Yang<sup>2</sup>, and Xiaocong Yuan<sup>1, 3, \*</sup>

<sup>1</sup>*Nanophotonics Research Centre, Institute of Microscale Optoelectronics & State Key Laboratory of Radio Frequency Heterogeneous Integration, Shenzhen University, Shenzhen 518060, China*

<sup>2</sup>*Research Institute of Interdisciplinary Science & School of Materials Science and Engineering, Dongguan University of Technology, Dongguan 523808, China*

<sup>3</sup>*Zhejiang Lab, Research Center for Humanoid Sensing, Research Institute of Intelligent Sensing, Hangzhou 311100, China*

<sup>#</sup>These authors contribute equally to the work.

\*Authors to whom correspondence should be addressed: [pittshiustc@gmail.com](mailto:pittshiustc@gmail.com), [lpdu@szu.edu.cn](mailto:lpdu@szu.edu.cn) and [xcyuan@szu.edu.cn](mailto:xcyuan@szu.edu.cn)

**Abstract:** Electromagnetic waves characterized by intensity, phase, and polarization degrees of freedom are widely applied in data storage, encryption, and communications. However, these properties can be substantially affected by phase disorders and disturbances, whereas high-dimensional degrees of freedom including momentum and angular momentum of electromagnetic waves can offer new insights into their features and phenomena, for example topological characteristics and structures that are robust to these disturbances. Here, we discover and demonstrate theoretically and experimentally spin–momentum locking and topological defects in unpolarized light. The coherent spin is locked to the kinetic momentum except for a small coupling spin term, due to the simultaneous presence of transverse magnetic and electric components in unpolarized light. To cancel the coupling term, we employ a metal film acting as a polarizer to form some skyrmion-like spin textures at the metal/air interface. Using an in-house scanning optical microscopic system to image the out-of-plane spin density of the focused unpolarized vortex light, we obtained experimental results that coincide well with our theoretical predictions. The theory and technique promote the applications of topological defects in optical data storage, encryption, and decryption, and communications.

## 1. Introduction

Momentum and angular momentum (AM), which are two fundamental dynamical properties of the electromagnetic (EM) field, play an important role in understanding and predicting light–matter interactions [1–4]. Generally, angular momentum can be decomposed into spin angular momentum (SAM) associated with circular polarization and orbital angular momentum (OAM) carried by the vortex phase [5]. The pairwise coupling of momentum, SAM, and OAM has resulted in a plenitude of remarkable phenomena, including the spin Hall effect of light [6,7], the optical Magnus effect [8], spin–orbit AM conversions [9,10], the quantum spin Hall effect of light [11–14], and optical topological defects [15–21]. It has led to the emergence of interesting research fields of optical spin–orbit interactions and offers

potential applications in manipulation [22–24], imaging [25,26], detection [27], metrology [28], data storage [29], encryption [30–35], and communications [36–38].

Previously, most of the research on optical spin–orbit interactions rely on pure polarized light, whereas the spin–orbit properties in a random or unpolarized field are rarely involved [39–41]. However, unpolarized fields are prevalent in optical data encoding, encryption, and free-space communications [30–38]. For example, consider encrypted structured light obtained by passing it through a random phase plate (RPP) with different Fresnel transmission coefficients and phase delays for the transverse electric (TE) and transverse magnetic (TM) polarization components respectively. The information encoded in the incident light by the intensity, phase, and polarization degrees of freedom is hard to be decrypted without auxiliary algorithms and keys because the transmission light is completely chaotic [35]. Nevertheless, the high-dimensional information in structured light [42], including the AM properties and the topological structure, can be protected even in the random EM system [43–45], which allows robust encryption and decryption in optical encryption systems and is also beneficial in applications in free-space optical communications.

In this work, we first demonstrate spin–momentum locking of unpolarized light, i.e., its coherent SAM density is locked with the Abraham–Poynting coherent kinetic momentum (KM) density even for focused unpolarized light, up to a small coupling term determined by the product of Fresnel transmission coefficients for the TM and TE-polarization components. This locking property satisfies the right-hand rule. Curiously, in contradiction with earlier results [39], an extraordinary axial SAM of unpolarized vortex light generated by passing linear polarized vortex light through a RPP establishes itself as the numerical aperture (NA) of objective lens increases. This makes it possible to form topological structures with unpolarized light. By utilizing a metal film to break the coupling between the TM- and TE-polarization components, various topological spin textures form at the metal/air interface. However, these topological spin textures are different from those produced by pure polarized light. We developed an in-house near-field optical scanning microscopic system to image the out-of-plane SAM densities of these topological spin textures. The experimental results match well with those from theory. The methods and techniques proposed here can be applied to the fields of robust optical data encoding, encryption, and communications based on topological defects.

## 2. Results

To begin, we consider monochromatic linear polarized light passing through a RPP for which the amplitude transmission coefficients and phase delays for TE and the TM polarized components are completely random [see Fig. 1(a)]. By calculating the degree of polarization  $\mathbb{P}$  and the complex degree of coherence  $\mathcal{M}_{12}$  of the transmission light at the plane  $H$ , we find that  $\mathbb{P} = 0$  and  $\mathcal{M}_{12} = 0$  simultaneously (see [Supplementary Note 1](#)). Thus, for the transmission light, its amplitude and phase are completely disordered, and the degree of polarization and the spatial coherence also vanish. Therefore, this transmission light can be considered as unpolarized light.

Nevertheless, the SAM density and KM density can be resolved because of the self-correlation property of this unpolarized light (see [Supplementary Note 2](#)). Here, we investigate the spin–momentum properties of this unpolarized light focused using an objective lens. After some lengthy calculations, we reached the conclusion that the coherent SAM density and KM density of this unpolarized light satisfy the relation (see [Supplementary Note 3](#)):

$$\mathbf{S} = \frac{1}{2k^2}(\nabla \times \mathbf{P}) + \mathbf{S}_c. \quad (1)$$

Here,  $\mathbf{S} = \text{Im}\{\varepsilon \mathbf{E}^* \times \mathbf{E} + \mu \mathbf{H}^* \times \mathbf{H}\}/4\omega$  is the SAM density; the KM density is  $\mathbf{P} = \text{Re}\{\mathbf{E}^* \times \mathbf{H}\}/2v^2$  with  $\mathbf{E}/\mathbf{H}$  denoting the electric/magnetic field,  $\varepsilon/\mu$  the permittivity/permeability of medium,  $\omega$  the angular frequency, and  $v$  the velocity of light in medium, respectively. The symbol  $\text{Re}/\text{Im}$  signifies the real/imaginary part of a complex number. This expression reveals that, even for unpolarized light, the spin is locked with the KM except for a very small term  $\mathbf{S}_c$  [see Fig. 1(b–d)]. This term  $\mathbf{S}_c$  represents the coupling between the TE and the TM polarized components because it is related to the product of the Fresnel transmission coefficients. Moreover, it is also determined by the numerical aperture (NA) of the objective lens. Therefore, to cancel or reduce this coupling term, one utilizes a polarizer to break the electric-magnetic dual symmetry or an objective lens with a small NA (see [Supplementary Figure 2](#)). In addition, Equation (1) suggests several methods to manipulate the SAM of unpolarized light: 1. The propagation direction can be controlled by adding an additional propagating phase to the incident light (because the spin is locked with the KM, the spin is inverted or inclined if the KM is reversed or tilted); and 2. The distribution of the KM density can be achieved by altering the EM modes or employing the multi-wave interference method (because the SAM density is proportional to the transverse gradient of the KM, the SAM density can be inverted or inclined by tuning the inhomogeneities of the KM density).

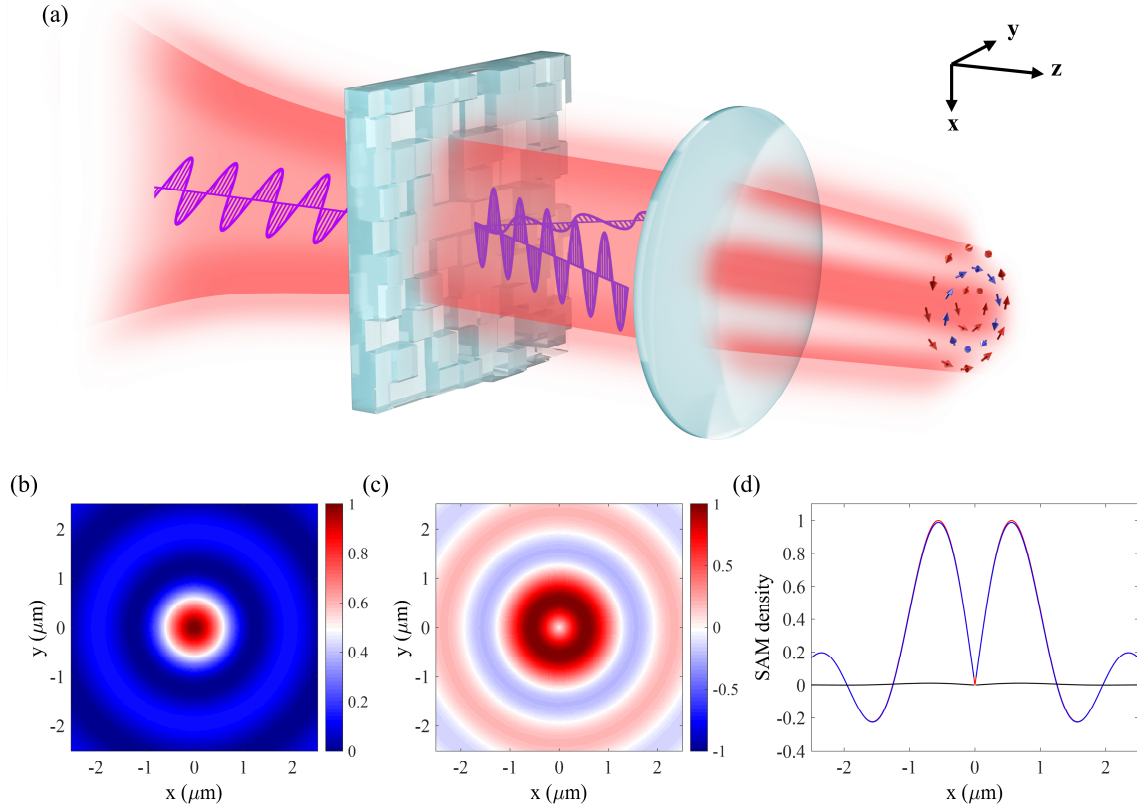


**Figure 1.** Spin–momentum locking of unpolarized light: (a) schematic of the generation of unpolarized light by passing linear polarized light through a RPP, which is subsequently focused by an objective lens; (b, c) density plots of the coherent KM and the coherent SAM density obtained with an objective lens of  $\text{NA} = 0.2$ , and (d) the one-dimensional (1D) contour plot of the total SAM density (red line), SAM density calculated using  $\nabla \times \mathbf{P}/2k^2$  (blue line), and the coupling SAM density  $\mathbf{S}_c$  (black line) indicate that, even for unpolarized light, spin is locked with KM except for a very small coupling term.

The optical vortex is widely applied in encoding and encryption applications [30–35]. Here, we also add a vortex phase with topological charge  $\ell$  to the incident linear-polarized light [Fig. 1(a)]. In this instance, spin–momentum locking given by Equation (1) is also fulfilled. Besides the axial KM density [Fig. 2(a)], the azimuthal KM density [Fig. 2(b)] is also present because of the vortex phase. Therefore, the radial gradient of the axial KM density leads to the emergence of an azimuthal SAM density [Fig. 2(c)], whereas the radial gradient of the azimuthal KM density leads to the appearance of the axial SAM density [Fig. 2(d)], which indicates that unpolarized light also possesses a three-dimensional spin vector required to construct the variety of photonic spin topological defects. In addition, because the axial SAM density is related to the azimuthal KM density, it can be manipulated using several methods: 1. The magnitude and direction of the azimuthal KM density can be controlled by the vortex topological charge  $\ell$ , because the azimuthal KM density is proportional to  $\ell$  (see [Supplementary Figure 5](#)); and 2. The magnitude of the axial SAM density is also related to the NA of objective lens because the orbit-to-spin AM conversion can be enhanced by enlarging the NA. For example, as the NA scales up from 0.2 to 0.8, the normalized axial SAM density also increases by two orders of magnitude (see [Supplementary Figure 4](#)).

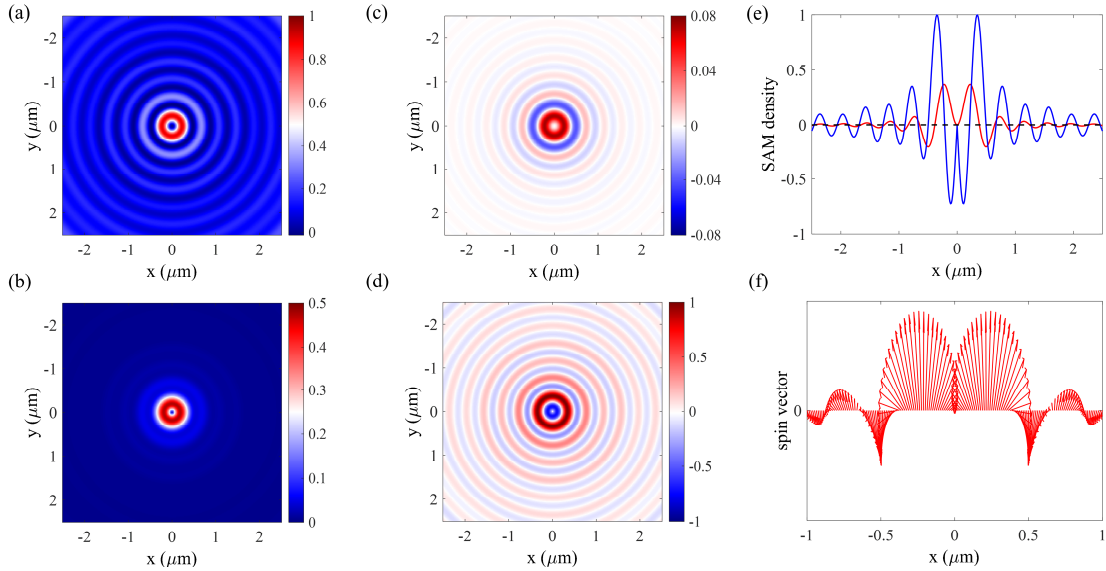


**Figure 2.** Spin–momentum properties and spin textures of focused unpolarized vortex light using an objective lens of NA = 0.8: (a) axial KM density and (b) azimuthal KM density of unpolarized light with vortex topological charge  $\ell = 1$ . According to the spin–momentum locking property, (c) the axial SAM density stems from the radial gradient of the azimuthal KM density, whereas (d) the azimuthal SAM density stems from the radial gradient of the axial KM density. From (e), the 1D contour of the SAM density (red line for the axial SAM density (the magnitude multiplied by 5) and blue line for the azimuthal SAM density), the null points of the axial SAM density and the azimuthal SAM density do not coincide, and thus the skyrmion number of (f) the spin texture formed by focused unpolarized vortex light is 0. The SAM density calculated from  $\nabla \times \mathbf{P}/2k^2$  (blue line) and the coupling SAM density  $\mathbf{S}_c$  (black line) indicate that, even for unpolarized light, the spin is locked with KM except for a tiny coupling term. Here, focused unpolarized vortex light is generated by passing linear polarized light through a RPP, which is subsequently focused by an objective lens.

On comparing topological spin textures constructed by the focused field of pure polarized vortex light [12–14], we find two primary differences between those textures formed by focused unpolarized vortex light and focused polarized light. First, the axial SAM density of focused unpolarized light exhibits a solid distribution when  $\ell = \pm 2$ , but has a donut shape for vortex topological charges taking other nonzero integer values (see [Supplementary Figure 5](#)). Second, the spin textures formed by focused unpolarized



light is topological trivial, indicating that the skyrmion number is 0 [Fig. 2(e, f)]. This trivial spin texture originates from the spatial incoherence of focused unpolarized light, because the coherence vanishes among the focused components along the  $\theta$ -direction ( $\theta$  the polar angle of spherical coordinates in focusing space). In addition, the coupling term  $S_c$  also affects the topological geometry of spin textures. For example, paraxial vortex light, which can be considered as weakly focused vortex light containing only one wavevector component, forms a half-skyrmion-like spin texture at the focal plane instead of a skyrmion-like spin texture [46].

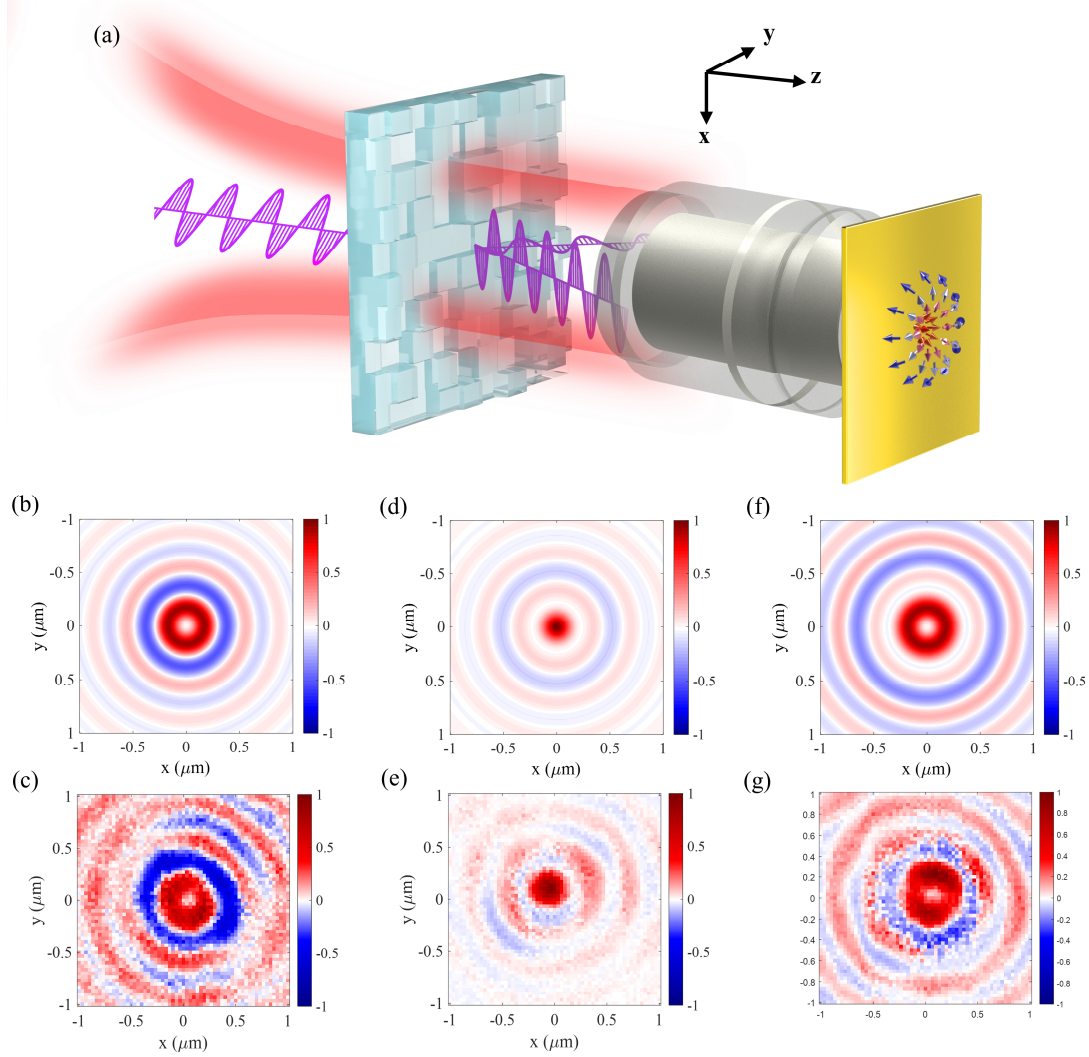


**Figure 3.** Photonic spin skyrmions formed in focused unpolarized vortex light: (a) schematic of the generation of photonic spin skyrmions in focused unpolarized vortex light. Linear polarized vortex light passes through a RPP and then is focused by an oil immersion objective lens with NA = 1.49 onto a metal surface. For an incident vortex of topological charge  $\ell = 1$ , (b) the theoretical and (c) the experimental axial SAM densities coincide strongly, verifying the photonic spin skyrmion formed by unpolarized light. (d, e) Same as (b, c) but with  $\ell = 2$  and (f, g) Same as (b, c) but with  $\ell = 3$ . The wavelength is 632.8 nm; the thickness of the gold film is 45 nm.

To overcome the two limitations, we use a high-NA oil immersion objective lens to focus the unpolarized vortex light onto a metal film [Fig. 3(a)]. Only the TM polarized component is known to satisfy the wavevector matching condition and excite the surface plasmon (SP) mode at the metal/air interface [47]. In this instance, the spin-momentum relation for these SP vortex modes is expressible as

(Supplementary Note 4)

$$\mathbf{S} = \frac{1}{2k^2} (\nabla \times \mathbf{P}) \quad (2)$$

because the metal film acts as a polarizer and the small coupling term vanishes. Equation (2) signifies that, even for the SP mode excited by unpolarized light, the total coherent SAM density is locked with the coherent KM density. Skyrmion-like spin textures may also form within focused unpolarized light. However, there are two differences between spin textures formed by polarized and unpolarized light. First, as with the SAM distributions of focused unpolarized light in free space, the axial SAM density displays a solid distribution when  $\ell = \pm 2$  [Fig. 3(d, e) for  $\ell = 2$ ], and forms a donut shape when the incident vortex takes topological charge of other nonzero integer values [Fig. 3(b, c) for  $\ell = 1$  and 3(f, g) for  $\ell = 3$ ]. Second, from the 1D contours of SAM densities (Supplementary Figure 5), one finds that, for  $\ell = 1$ , the skyrmion-like spin texture forms in the center. The skyrmion number can be calculated from

$$n_{sk} = \frac{1}{4\pi} \iint \mathbf{M} \cdot \left( \frac{\partial \mathbf{M}}{\partial x} \times \frac{\partial \mathbf{M}}{\partial y} \right) dx dy = -\frac{1}{2} \int_{r_n}^{r_{n+1}} M_r \left( M_r \frac{\partial M_z}{\partial r} - \frac{\partial M_r}{\partial r} M_z \right) dr, \quad (3)$$

where  $\mathbf{M} = [M_r, 0, M_z]^T$  denotes the normalized spin vector ( $\mathbf{M} = \mathbf{S}/|\mathbf{S}|$ ); superscript T signifies the transpose of matrix. For example, the skyrmion topological number of a spin texture from the center to the first approximate null point of the radial SAM density ( $r_0 = 0$  and  $r_1 = 495.2\text{nm}$ ) is  $n_{sk} = 1$ . For  $\ell > 1$ , no skyrmion-like spin texture is formed in the center. The reason lies in the expressions in Supplementary Equations (S64–S66), which reveal that the coefficients of the term containing  $J_{\ell-1}$  and  $J_{\ell+1}$  are non-vanishing and these two functions do not possess the same null points at small radial values. Here, the symbol  $J$  signifies a Bessel function of the first kind. For large radial values,  $J_{n-1}(r) \approx \cos(r - (2n-1)\pi/4)$ , and thus  $J_{n+1}(r) \approx \cos(r - (2n+3)\pi/4) = -\cos(r - (2n-1)\pi/4)$ . In this instance, the null points of the terms containing  $J_{\ell-1}$  and  $J_{\ell+1}$  coincide and a skyrmion-like spin texture forms.

To validate the intriguing hidden spin–momentum locking and topological defects in a focused unpolarized field, we developed a scanning imaging system to map the out-of-plane SAM densities of the topological spin skyrmions (see Supplementary Figure 7; details of the experiment are given in Supplementary Note 5). Figure 3(b, d, f) plots the results calculated from theory of out-of-plane SAM densities for incident vortex light with vortex topological charge  $\ell = 1, 2, 3$ . The corresponding experimental results are presented in Fig. 3(c, e, g). In addition, the experimental results of out-of-plane SAM densities for incident vortex light with vortex topological charge  $\ell = 4$  to 10 are given in Supplementary Figure 8. These results show that the distribution of the SAM density possesses a solid distribution at  $\ell = 2$  and in the other cases ( $\ell$  a positive integer with  $\ell \neq 2$ ) are hollow. The experimental results agree well with the theoretical results, thus demonstrating the validity of our theory.

**Discussions and conclusions:** To summarize, we first discover and demonstrate theoretically and experimentally spin–momentum locking of unpolarized light, i.e., the coherent SAM density is locked with the coherent KM density except for a small coupling term. This term appears with the simultaneous presence of TM and TE polarized components in unpolarized light. Therefore, by employing a metal film acting as a polarizer, we conclude that the total SAM density is locked with the KM density. By adding a vortex phase to the incident light, skyrmion-like spin textures form at the metal/air interface. Interestingly, by comparing the skyrmion-like spin textures formed by focused polarized light, the distributions of spin

textures formed by focused unpolarized light have two significant features: 1) the axial SAM density has a solid distribution when the vortex topological charge is  $\ell = \pm 2$  and possesses a donut shape for other nonzero integers; and 2), apart from  $\ell = \pm 1$ , the skyrmion-like spin textures only form at large radial values whereas the skyrmion topological number is zero for spin textures in the center. On the experimental side, we developed an in-house near-field optical scanning microscopic system to image the out-of-plane SAM densities of these topological spin textures. The experimental results match well with the theoretical results, thus validating our theory. The theory and technique proposed here can be applied to the fields of robust optical data encoding, encryption, and communications based on topological defects.

### Acknowledgements

This work was supported, in part, by the Guangdong Major Project of Basic Research grant 2020B0301030009, the National Natural Science Foundation of China grants 12174266, 92250304, 61935013, 62075139, 61427819, 61622504, 12004260, the Leadership of Guangdong province program grant 00201505, and the Science and Technology Innovation Commission of Shenzhen grants JCYJ20200109114018750.

### Author contributions

All authors contributed to the article.

### Competing interests

The authors declare no competing interests.

### Data availability

The data that support the plots within this paper and other findings of this study are available from the corresponding author upon reasonable request.

### References:

- [1] Bliokh, K. Y. Rodríguez-Fortuño, F. J., Nori, F., and Zayats, A. V. Spin-orbit interactions of light. [Nat. Photon.](#) 9(12), 796–808 (2015).
- [2] Aiello, A., Banzer, P., Neugebauer, M., and Leuchs, G. From transverse angular momentum to photonic wheels. [Nat. Photon.](#) 9(12), 789–795 (2015).
- [3] Shi, P., Yang, A., Meng, F., Chen, J., Zhang, Y., Xie, Z., Du, L., and Yuan, X. Optical near-field measurement for spin-orbit interaction of light. [Prog. in Quantum Electron.](#) 78, 100341 (2021).
- [4] Shi, P., Du, L., and Yuan, X. Spin photonics: from transverse spin to photonic skyrmions. [Nanophotonics](#) 10, 3927-3943 (2021).
- [5] Shen, Y. *et al.* Optical vortices 30 years on: OAM manipulation from topological charge to multiple singularities. [Light Sci. Appl.](#) 8, 90(2019).
- [6] Bliokh, K. Y. and Bliokh, Y. P. Conservation of angular momentum, transverse shift, and spin Hall effect in reflection and refraction of an electromagnetic wave packet. [Phys. Rev. Lett.](#) 96, 073903 (2006).
- [7] Ling, X., Zhou, X., Huang, K., Liu, Y., Qiu, C.-W., Luo, H., and Wen, S. Recent advances in the spin Hall effect of light. [Rep. Prog. Phys.](#) 80, 066401 (2017).
- [8] Bliokh, K. Y., Niv, A., Kleiner, V., and Hasman, E. Geometrodynamics of spinning light. [Nat. Photon.](#) 2, 748–753 (2008).

- [9] Zhao, Y., Edgar, J. S., Jeffries, G. D. M., McGloin, D. & Chiu, D. T. Spin-to-orbital angular momentum conversion in a strongly focused optical beam. *Phys. Rev. Lett.* 99, 073901 (2007).
- [10] Neugebauer, M., Eismann, J. S., Bauer, T., and Banzer, P. Magnetic and electric transverse spin density of spatially confined light. *Phys. Rev. X* 8, 021042 (2018).
- [11] Bliokh, K. Y., Smirnova, D. & Nori, F. Quantum spin Hall effect of light. *Science* 348, 1448–1451 (2015).
- [12] Shi, P., Du, L., Li, C., Zayats, A. V., and Yuan, X. Transverse spin dynamics in structured electromagnetic guided waves. *Proc. Natl. Acad. Sci. USA*. 118(6), e2018816118 (2021).
- [13] Shi, P., Lei, X., Zhang, Q., Li, H., Du, L., and Yuan, X. Intrinsic spin-momentum dynamics of surface electromagnetic waves in dispersive interfaces. *Phys. Rev. Lett.* 128, 213904 (2022).
- [14] Shi, P., Yang, A., Yin, X., Du, L., Lei, X., and Yuan, X. Spin decomposition and topological properties in a generic electromagnetic field, accepted by *Commun. Phys.* (2023). DOI: <https://doi.org/10.1038/s42005-023-01374-y>
- [15] Tsesses, S., Cohen, K., Ostrovsky, E., Gjonaj, B., and Bartal, G. Spin-orbit interaction of light in plasmonic lattices. *Nano Lett.* 19, 4010-4016 (2019).
- [16] Dai, Y., Zhou, Z., Ghosh, A., Mong, R. S. K., Kubo, A., Huang, C.-B., and Petek, H. Plasmonic topological quasiparticle on the nanometre and femtosecond scales. *Nature* 588, 616-619 (2020).
- [17] Li, C., Shi, P., Du, L., and Yuan, X. Mapping the near-field spin angular momenta in the structured surface plasmon polariton field. *Nanoscale* 12, 13674-13679 (2020).
- [18] Ghosh, A., Yang, S., Dai, Y., Zhou, Z., Wang, T., Huang, C., and Petek, H. A topological lattice of plasmonic merons. *Appl. Phys. Rev.* 8, 041413 (2021).
- [19] Shi, P., Du, L., and Yuan, X. Strong spin-orbit interaction of photonic skyrmions at the general optical interface. *Nanophotonics* 9(15), 4619-4628 (2020).
- [20] Dai, Y., Zhou, Z., Ghosh, A., Kapoor, K., Dąbrowski, M., Kubo, A., Huang, C.-B., and Petek, H. Ultrafast microscopy of a twisted plasmonic spin skyrmion. *Appl. Phys. Rev.* 9, 011420 (2022).
- [21] Lei, X., Yang, A., Shi, P., Xie, Z., Du, L., Zayats, A. V., and Yuan, X. Photonic spin lattices: symmetry constraints for skyrmion and meron topologies. *Phys. Rev. Lett.* 127, 237403 (2021).
- [22] Yu, X., Li, Y., Xu, B., Wang, X., Zhang, L., Chen, J., Lin, Z., and Chan, C.-T. Anomalous lateral optical force as a manifestation of the optical transverse spin. *Laser Photonics Rev.* 17(9), 202300212 (2023).
- [23] Shi, Y., Zhu, T., Liu, J., Tsai, D.-P., Zhang, H., Wang, S., Chan, C.-T., Wu, P.-C., Zayats, A. V., Nori, F., and Liu, A.-Q. Stable optical lateral forces from inhomogeneities of the spin angular momentum. *Sci. Adv.* 8(48), abn2291 (2022).
- [24] Rodríguez-Fortuño, F. J., Engheta, N., Martínez, A., and Zayats, A. V. Lateral forces on circularly polarizable particles near a surface. *Nat. Commun.* 6, 8799 (2015).
- [25] Zhou, J. *et al.* Metasurface enabled quantum edge detection, *Sci. Adv.* 6(51), eabc4385(2020).
- [26] Zhou, J. *et al.* Optical edge detection based on high-efficiency dielectric metasurface, *Proc. Natl. Acad. Sci. USA*. 116(23), 11137-11140(2019).
- [27] Lei, X., Du, L., Yuan, X., and Zayats, A. V. Optical spin-orbit coupling in the presence of magnetization: photonic skyrmion interaction with magnetic domains, *Nanophotonics* 10(14), 3667–3675(2021).
- [28] Yang, A. *et al.* Spin-manipulated photonic skyrmion-pair for pico-metric displacement sensing, *Adv. Sci.* 10(12), 2205249 (2023).
- [29] Ouyang, X., Xu, Y., Xian, M. *et al.* Synthetic helical dichroism for six-dimensional optical orbital angular momentum multiplexing. *Nat. Photon.* 15, 901–907 (2021).
- [30] Yang, H., He, P., Ou, K. *et al.* Angular momentum holography via a minimalist metasurface for optical nested encryption. *Light Sci. Appl.* 12, 79 (2023).

- [31] Liu, S., Wang, X., Ni, J., Cao, Y., Li, J., Wang, C., Hu, Y., Chu, J., and Wu, D. Optical Encryption in the Photonic Orbital Angular Momentum Dimension via Direct-Laser-Writing 3D Chiral Metahelices. *Nano Lett.* 23(6) 2304–2311 (2023).
- [32] Fang, X., Ren, H., and Gu, M. Orbital angular momentum holography for high-security encryption. *Nat. Photon.* 14, 102–108 (2020).
- [33] Ren, H., Fang, X., Jang, J. et al. Complex-amplitude metasurface-based orbital angular momentum holography in momentum space. *Nat. Nanotechnol.* 15, 948–955 (2020).
- [34] Qu, G., Yang, W., Song, Q. et al. Reprogrammable meta-hologram for optical encryption. *Nat. Commun.* 11, 5484 (2020).
- [35] Alfalou, A. and Brosseau, C. Optical image compression and encryption methods. *Adv. Opt. Photon.* 1, 589–636 (2009).
- [36] Lin, Z., Hu, J., Chen, Y., Brès, C., and Yu, S. Single-shot Kramers–Kronig complex orbital angular momentum spectrum retrieval. *Adv. Photon.* 5(3), 036006 (2023).
- [37] Lei, T., Zhang, M., Li, Y. et al. Massive individual orbital angular momentum channels for multiplexing enabled by Damman gratings. *Light Sci. Appl.* 4, e257 (2015).
- [38] Wang, J., Yang, JY., Fazal, I. et al. Terabit free-space data transmission employing orbital angular momentum multiplexing. *Nat. Photon.* 6, 488–496 (2012).
- [39] Eismann, J.S., Nicholls, L.H., Roth, D.J. et al. Transverse spinning of unpolarized light. *Nat. Photon.* 15, 156–161 (2021).
- [40] Chen, Y., Wang, F., Dong, Z., Cai, Y., Norrman, A., Gil, J. J., Friberg, A. T., and Setälä, T. Structure of transverse spin in focused random light. *Phys. Rev. A* 104, 013516 (2021).
- [41] Chen, Y., Norrman, A., Ponomarenko, S. A., and Friberg, A. T. Spin density in partially coherent surface-plasmon-polariton vortex fields. *Phys. Rev. A* 103, 063511 (2021).
- [42] He, C., Shen, Y. & Forbes, A. Towards higher-dimensional structured light. *Light Sci. Appl.* 11, 205 (2022).
- [43] Liu, C., Zhang, S., Maier, S. A., and Ren, H. Disorder-induced topological state transition in the optical skyrmion family. *Phys. Rev. Lett.* 129, 267401 (2022).
- [44] Shi, P., Du, L., Li, M., and Yuan, X. Symmetry-protected photonic chiral spin textures by spin-orbit coupling. *Laser Photonics Rev.* 15, 202000554 (2021).
- [45] Shi, P., Zhang, Q., and Yuan, X. Topological state transitions in electromagnetic topological defects. <https://doi.org/10.48550/arXiv.2306.12024> (2023).
- [46] Shi, P., Li, H., Du, L., and Yuan, X. Spin-momentum properties in the paraxial optical systems. *ACS Photon.* 10, 2332–2343 (2023).
- [47] Du, L., Yang, A., Zayats, A. V. and Yuan, X. Deep-subwavelength features of photonic skyrmions in a confined electromagnetic field with orbital angular momentum. *Nat. Phys.* 15, 650–654 (2019).